

Figure 2. Pancreatitis is ameliorated in cerulein-administered CCL2^{-/-} mice. (A) H&E staining of the pancreas in cerulein-administered WT and CCL2^{-/-} mice. Original magnification, $\times 200$. (B) Histological scores (n = 5). * $P < .05$. (C) Serum amylase and lipase levels (n = 10). * $P < .05$. (D) Expression of CD11b/Gr-1 on pancreatic cells of the indicated mice administered cerulein. (E) Absolute cell numbers of each subpopulation (n = 4) of the indicated mice administered cerulein. * $P < .05$. (F) Mean fluorescence intensities of CD80 and CD86 on each subpopulation (n = 4) of the indicated mice administered cerulein. Data are representative of 2 independent experiments. MFI, mean fluorescent intensity; n.s., not significant.

the pancreas, while both mice in group 2 showed equally inflammatory pathology in the pancreas (Figure 3B). Surprisingly, however, only the injected mice of group 3 parabionts showed pathological findings (Figure 3B). Consistently, the concentrations of serum amylase and lipase in group 2 and group 3 were significantly higher than those in group 1, and those in group 2 were almost double those in group 3, although the difference was not significant (Figure 3C). Furthermore, the absolute cell numbers of the S2 and S3 subpopulations in the pancreas of the cerulein-administered parabionts, but not the PBS-administered parabionts, in group 2 and group 3 were significantly higher than those in group 1 (Figure 3D and E). However, no significant differences in the absolute cell numbers of the S1 subpopulation were found between any of the 3 groups (Figure 3D and E). These surprising results indicated that the disease occurs in the injected parabionts only, despite the active circulation of immune cells, suggesting that the mechanism of pancreas damage involves direct translation of cerulein from the peritoneal cavity to the pancreas. To further assess the hemodynamics of the S1, S2, and S3 subpopulations after cerulein injection, we separately assessed host- and donor-derived cells by staining the Ly5.1 and Ly5.2 markers. Consistent with these findings, the homing of donor-derived cells of

the S1 and S2 subpopulations was highly restricted at approximately 1:9 to 2:8 compared with that of S3 cells (approximately 1:3) (Figure 3F), although the numbers of S2 and S3 cells were increased by almost 70-fold after cerulein injection (Figure 3E).

To further assess the role of the CCR2/CCL2 axis in the pathogenesis of this model, we again performed parabiosis surgery between Ly5.1⁺ WT and Ly5.2⁺ CCL2^{-/-} mice, and injected both mice with cerulein at 2 weeks after the surgery (Supplementary Figure 6A). Consistent with the previous data, CCL2^{-/-} mice developed less severe pancreatitis than WT mice (Supplementary Figure 6B) in accordance with the lower infiltration of S2 cells into CCL2^{-/-} mice, but comparable infiltration of S3 cells (Supplementary Figure 6C and D). Furthermore, irrespective of the diseased WT mice or nondiseased CCL2^{-/-} mice, the percentages of chimerism were <20% in the S1 and S2 subpopulations and <30% in the S3 subpopulation (Supplementary Figure 6C and D), suggesting that the infiltrating cells were derived from some reservoirs on the host side.

Given the finding that the pancreatitis only occurred in the cerulein-injected parabionts in the parabiosis system, we hypothesized that cerulein damages the pancreas, leading to up-regulation of chemokine expression, and then

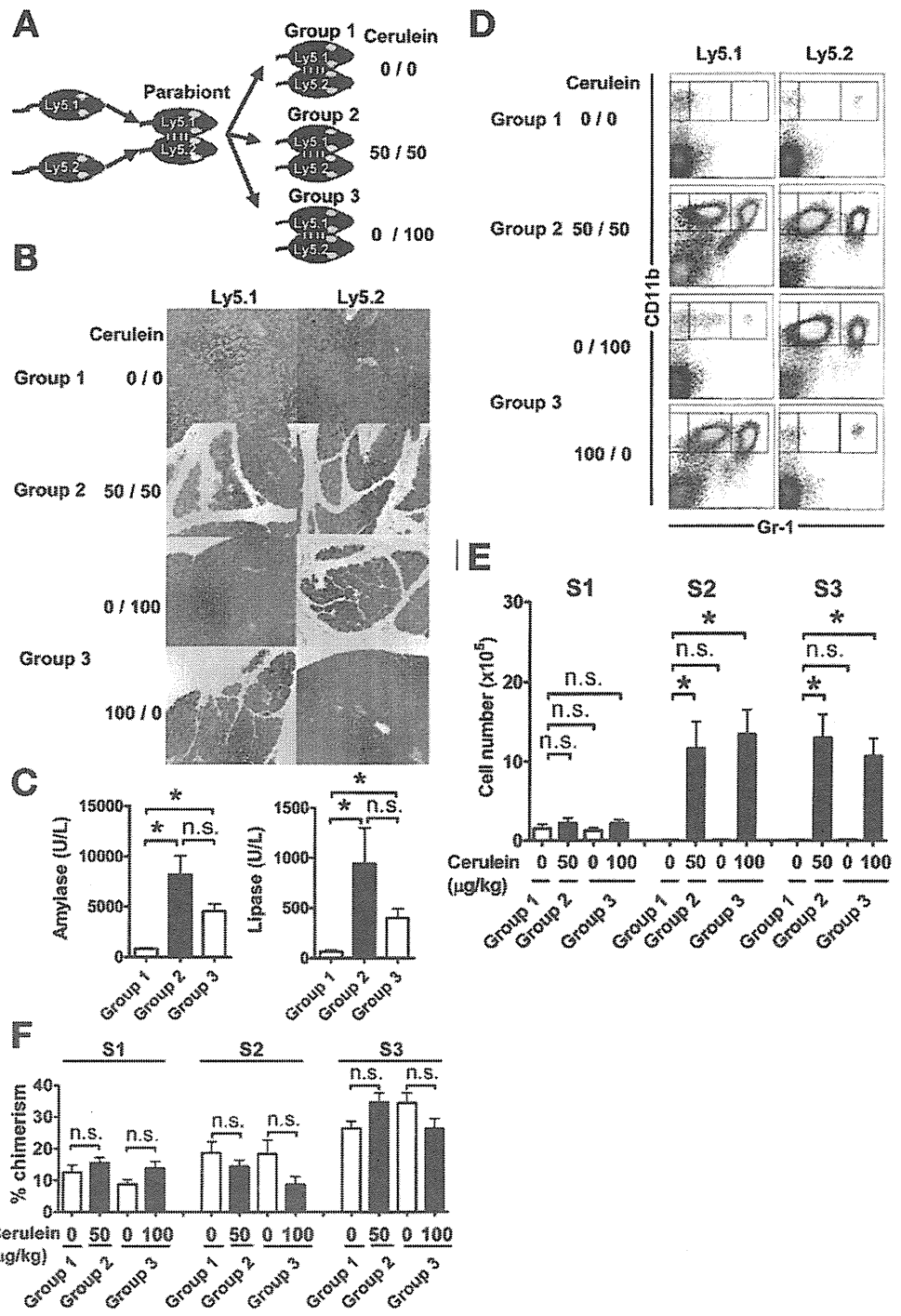


Figure 3. Hemodynamics of pancreatic mononuclear cells. (A) Study design. Parabionts were divided into 3 groups. Group 1 (6 pairs), not administered cerulein; group 2 (6 pairs), 50 $\mu\text{g}/\text{kg}$ cerulein bilaterally; group 3 (6 pairs), 100 $\mu\text{g}/\text{kg}$ cerulein to only 1 partner. (B) H&E staining of the pancreas. Original magnification, 200 \times . (C) Serum amylase and lipase levels. * $P < .05$. (D) Flow cytometry of CD11b/Gr-1. Data are representative of at least 5 independent experiments. (E) Absolute cell numbers of each subpopulation. * $P < .05$. (F) Percentages of chimerism of each subpopulation in each group. n.s., not significant.

macrophages/granulocytes/MDSCs in reservoirs migrate to the diseased pancreas. Therefore, we focused on the bone marrow (BM) as a reservoir for migratory macrophages in this model.²² As expected, the absolute cell number of the CD11b^{high}Gr-1^{low} S2 subpopulation, but not the other subpopulations, in the BM of cerulein-administered mice was significantly lower than that in PBS-administered mice (Supplementary Figure 7). These findings indicate that S2 cells in the BM are mobilized into the injured pancreas after cerulein injection.

Suppressor of Cytokine Signaling 3–Mediated Activation of Macrophages Is Involved in Development of Cerulein-Induced Pancreatitis

Although these results clearly demonstrated that CCR2/CCL2-mediated migration of S2 macrophages to the pancreas is critically involved in the pathogenesis of cerulein-induced pancreatitis, surprisingly, the expression levels of CD80 and CD86 on S1, S2, and S3 cells in the pancreas of cerulein-injected CCL2^{-/-} mice were up-regulated and comparable with those in the pancreas of

BASIC AND TRANSLATIONAL PANCREAS

cerulein-injected WT mice (Figure 2*F*). This was also the case for cerulein-administered RAG-2^{-/-} mice, which showed marked infiltration of S2 and S3 cells and up-regulation of CD80 and CD86 costimulatory molecules (Supplementary Figure 1*D–F*). These observations suggest that the macrophage activation step (step 2) in the cerulein-injected pancreas is involved in this model, in addition to the macrophage migration step (step 1). Regarding this issue, it was interesting that only interleukin (IL)-6, unlike other proinflammatory cytokines, is protective in this model.²³ It is well known that signal transducer and activation of transcription (STAT)3 activation by IL-6 inhibits nuclear factor- κ B (NF- κ B) activation, and conversely suppressor of cytokine signaling (SOCS) 3 suppresses STAT3 activation via IL-6.²⁴ Therefore, we hypothesized that SOCS3 is critically involved in step 2, the activation of pancreatic macrophages, in this model.

We confirmed that SOCS3 was specifically deleted in CD11b⁺, but not CD11b⁻, cells isolated from the pancreas of macrophage-specific SOCS3-conditional knockout (SOCS3cKO) mice (Supplementary Figure 8*A*). Consistent with our hypothesis, TNF- α production from splenic lipopolysaccharide (LPS)-stimulated SOCS3cKO CD11b⁺ cells was significantly lower than that from splenic LPS-stimulated WT CD11b⁺ cells, while IL-10 production from splenic LPS-stimulated SOCS3cKO CD11b⁺ cells was significantly higher than that from splenic LPS-stimulated WT CD11b⁺ cells (Supplementary Figure 8*B*). Interestingly, however, IL-6 production was not affected by the deletion of SOCS3 in CD11b⁺ cells (Supplementary Figure 8*B*). Furthermore, importantly, the messenger RNA of SOCS3 in pancreatic CD11b⁺Gr-1^{low} S2 cells from cerulein-injected mice was significantly higher than that from PBS-injected mice, and the messenger RNA of SOCS1 was not affected by the cerulein injection (Supplementary Figure 8*C*).

To further test this hypothesis, we compared age-matched WT and SOCS3cKO mice in this cerulein model. Histological analyses revealed that cerulein-administered SOCS3cKO mice developed significantly milder pancreatitis than control WT mice, based on the histological scores (Figure 4*Ai* and *Aii*). Consistently, the serum concentrations of amylase and lipase in cerulein-administered SOCS3cKO mice were significantly lower than those in control WT mice (Figure 4*B*). The ratios and absolute cell numbers of the S1, S2, and S3 subpopulations were comparable in the 2 groups (Figure 4*C*). In contrast, the up-regulation of CD80 and CD86 on S1 and S2 macrophages, but not on S3 granulocytes/MDSCs, in the pancreas was significantly impaired in cerulein-administered SOCS3cKO mice compared with cerulein-injected WT mice (Figure 4*D*).

Notably, the expression of TNF- α , but not IL-10, in the S1 and S2 subpopulations of pancreatic mononuclear cells from cerulein-injected SOCS3cKO mice after culture in the presence or absence of LPS was markedly impaired compared with paired cells from cerulein-injected WT mice (Figure 4*Ei* and *Eii*). In contrast, the S3 granulocyte/MDSC subpopulations from both WT and SOCS3cKO

mice expressed IL-10, but not TNF- α , regardless of culture in the presence or absence of LPS (Figure 4*Ei* and *Eii*), suggesting that this population includes IL-10-expressing MDSCs in addition to granulocytes. Consistent with these results, the phosphorylation of STAT3, but not p38 mitogen-activated protein kinase, in S2 macrophages in the pancreas of cerulein-administered mice was significantly higher than that in the pancreas of PBS-administered mice (Figure 4*Fi* and *Fii*). In a similar experiment using macrophage-specific SOCS1-cKO mice, cerulein-administered WT mice and SOCS1cKO mice similarly developed pancreatitis and showed no detectable significant differences (Supplementary Figure 9*A–F*).

CCR2/CCL2-Mediated Migration of Macrophages Is Involved in Development of L-Arg-Induced Acute Pancreatitis

We further assessed whether the 2-step model (migration and activation of macrophages) is generally accepted in other murine models of acute pancreatitis. To this end, we used an L-Arg-induced acute pancreatitis model.²⁵ We confirmed the presence of acute pancreatitis accompanied by marked acinar cell damage and infiltration of mononuclear cells (Supplementary Figure 10*A*) and higher serum levels of amylase and lipase (Supplementary Figure 10*B*) in L-Arg-injected mice. Similar to the cerulein model, the ratio and absolute number of the CD11b⁺Gr-1^{low} S2 subpopulation were markedly increased in the L-Arg model, whereas, unlike the cerulein model, the ratio and absolute number of the CD11b⁺Gr-1⁻ S1 subpopulation were also significantly increased in the L-Arg model, while the ratio and absolute number of the CD11b⁺Gr-1^{high} S3 subpopulation were comparable (Figure 5*Ai* and *Aii*). Consistent with the cerulein model, the expression levels of CD80 and CD86 on S1, S2, and S3 cells in the pancreas of L-Arg-injected mice were significantly up-regulated compared with those in the pancreas of PBS-injected WT mice (Figure 5*B*).

Next, we compared WT and CCL2^{-/-} mice in the L-Arg model. As expected, CCL2^{-/-} mice were resistant to the model compared with WT mice based on the histology (Figure 5*Ci*) and serum levels of amylase and lipase (Figure 5*Cii*). The absolute numbers of S1 and S2, but not S3, cells in the pancreas of L-Arg-injected CCL2^{-/-} mice were significantly lower compared with WT mice (Figure 5*Di* and *Dii*), while the expression levels of CD80 and CD86 on S1, S2, and S3 cells after L-Arg injection were comparable in the 2 groups (Figure 5*E*). Furthermore, we compared WT and SOCS3cKO mice using the L-Arg model. L-Arg-injected SOCS3cKO mice tended to develop mild pancreatitis compared with L-Arg-injected WT mice in terms of the histology and serum concentrations of amylase and lipase, although the differences were not significant (Supplementary Figure 11*A* and *B*).

Discussion

In this study, we have demonstrated sequential steps of macrophage migration and activation in the pathogenesis of cerulein-induced acute pancreatitis: step 1, CCL2/CCR2-

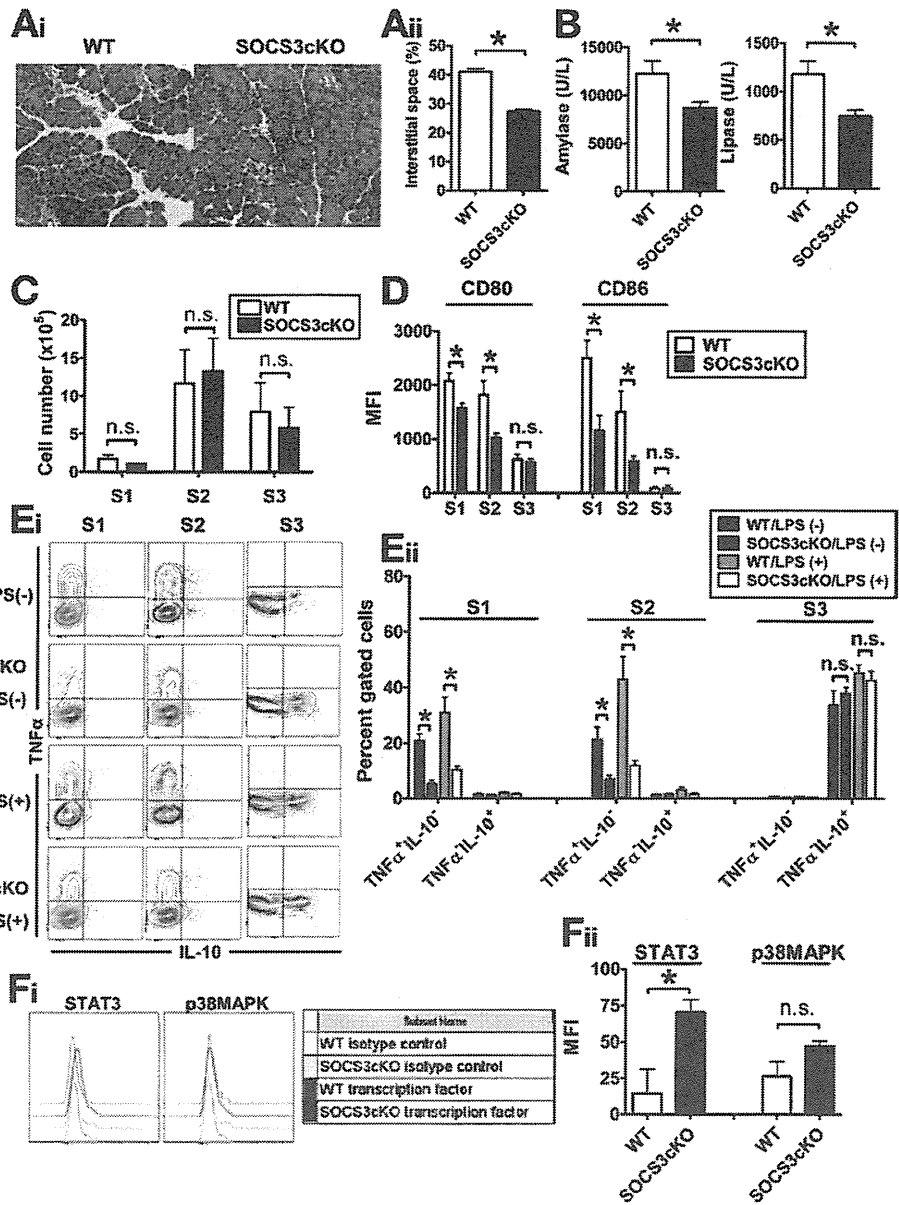


Figure 4. SOCS3 in pancreatic macrophages promotes activation of pancreatic macrophages and enhances the severity of pancreatitis. (A) H&E staining of the pancreas in cerulein-administered WT and SOCS3cKO mice. Original magnification, $\times 200$. (Aii) Histological scores ($n = 9$). $*P < .05$. (B) Serum amylase and lipase levels ($n = 9$). $*P < .05$. (C) Absolute cell numbers of the CD11b⁺Gr-1⁻ S1, CD11b⁺Gr-1^{low} S2, and CD11b⁺Gr-1^{high} S3 pancreatic subpopulations ($n = 3$). (D) Mean fluorescence intensities of CD80 and CD86 on pancreatic cells ($n = 3$). $*P < .05$. (E) Intracellular TNF- α and IL-10 expression with or without LPS stimulation in each subpopulation ($n = 4$). Data are representative of 2 independent experiments. (Eii) Percentages of the indicated cells in each subpopulation. $*P < .05$. (F) Flow cytometry of STAT3 and p38 mitogen-activated protein kinase phosphorylation in pancreatic S2 macrophages ($n = 4$). (Fii) Percentages of phosphorylation in the S2 subpopulation ($n = 4$). $*P < .05$. MAPK, mitogen-activated protein kinase; MFI, mean fluorescent intensity; n.s., not significant.

dependent migration of CD11b^{high}Gr-1^{low} macrophages to the damaged pancreas; and step 2, SOCS3-dependent activation of these macrophages. Thereafter, the activated macrophages might cross talk with still-unidentified acquired immune cells, instructing them to become the eventual effector cells that establish acute pancreatitis.¹³ Our immunological scenario for the development of cerulein-induced acute pancreatitis is depicted in Figure 6.

First, we comprehensively analyzed the compartments of immune cells in the pancreas by comparing them under steady-state conditions and during inflammation induced by cerulein administration. Contrary to our expectations, we found that almost all sets of immune compartments for innate and acquired immunity, such as APCs (cDCs and macrophages) and T, NKT, and NK cells, except for the CD11b^{high}CD11c⁻ population, resided in the normal pancreas. These findings suggest that the

immune system might be normally engaged in the maintenance of the pancreas, unlike previous physiological and biochemical visions for the maintenance of pancreatic homeostasis.

Consistent with this view, Demols et al¹³ demonstrated that T-cell-deficient *nu/nu* mice do not develop cerulein-induced pancreatitis, and concluded that this model is T-cell-dependent. In this regard, we confirmed that RAG-2^{-/-} mice were resistant to the cerulein model (Supplementary Figure 1). Although these results suggest that T cells are the eventual effectors that establish the pathogenesis of cerulein-induced acute pancreatitis, such hyperacute establishment of this disease seems to be more largely caused by the involvement of innate immune cells, which promptly produce effector cytokines, rather than the involvement of antigen-specific conventional TCR $\gamma\delta$ ⁺ T cells. Based on this hypothesis, we assessed the role of

BASIC AND TRANSLATIONAL PANCREAS

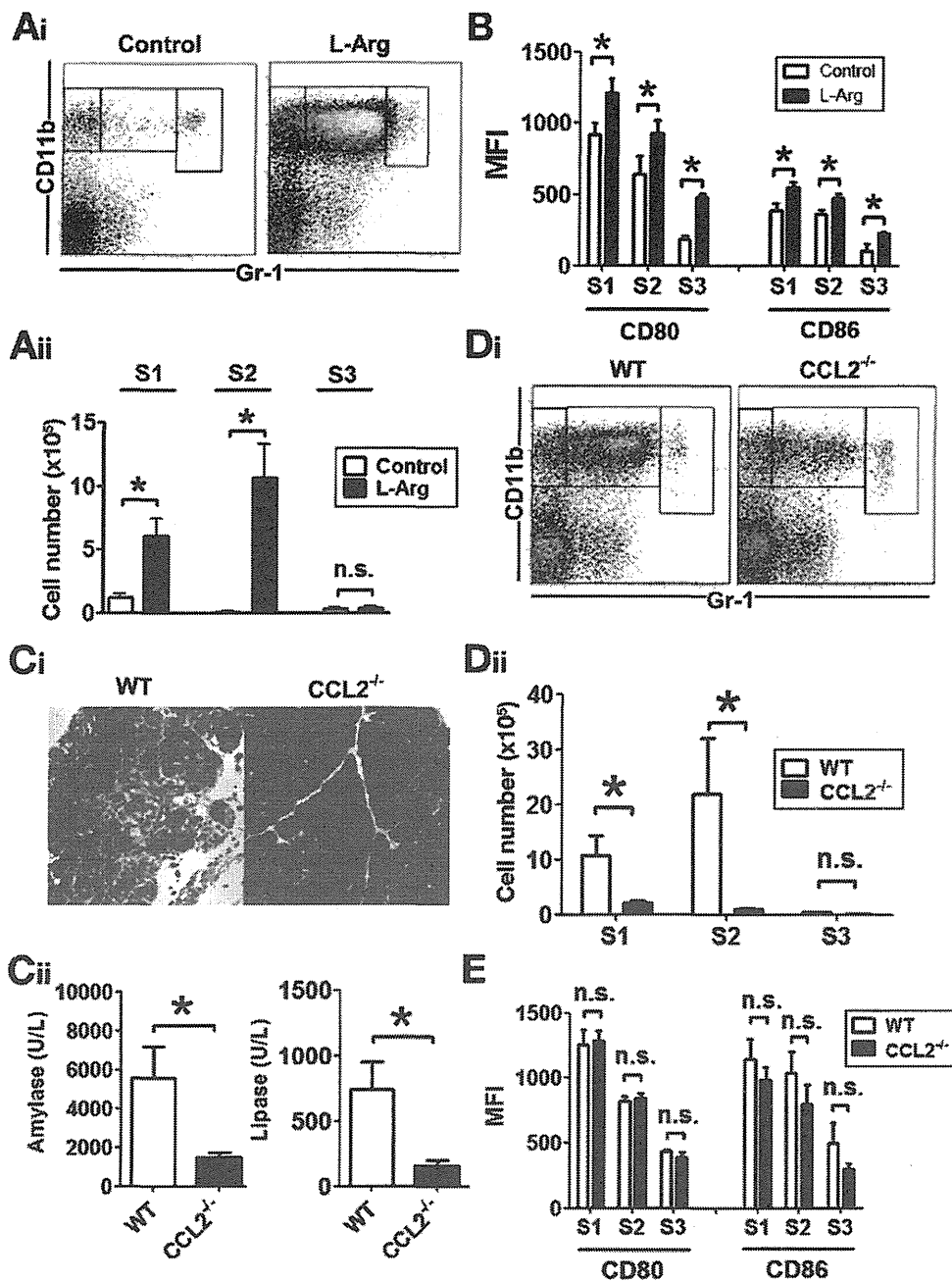


Figure 5. L-Arg-induced acute pancreatitis is mediated by CCL2/CCR2-mediated migration of macrophages. (Ai) Expression of CD11b/Gr-1 of cells isolated from the pancreas of L-Arg-injected (right) and saline-injected (left) mice. The boxes indicate: S1, CD11b^{high}Gr-1⁻; S2, CD11b^{high}Gr-1^{low}; and S3, CD11b^{high}Gr-1^{high}. (Aii) Absolute cell numbers of the 3 subpopulations in the pancreas of saline- or L-Arg-administered mice. Data are mean \pm standard error of mean (SEM) ($n = 4$ /group). * $P < .05$. (B) Mean fluorescence intensities of CD80 and CD86 on the 3 subpopulations. Data are representative of at least 4 independent experiments. Data are mean \pm SEM ($n = 4$ /group). * $P < .05$. (Ci) H&E staining of the pancreas in L-Arg-administered WT and CCL2^{-/-} mice. Original magnification, $\times 200$. (Cii) Serum amylase and lipase levels ($n = 5$). * $P < .05$. (Di) Expression of CD11b/Gr-1 on pancreatic cells of the indicated mice administered L-Arg. (Dii) Absolute cell numbers of each subpopulation ($n = 5$) of the indicated mice administered L-Arg. * $P < .05$. (E) Mean fluorescence intensities of CD80 and CD86 on each subpopulation ($n = 5$) of the indicated mice administered L-Arg. MFI, mean fluorescent intensity; n.s., not significant.

TCR $\gamma\delta^+$ T and NKT cells, which are deleted in RAG-2^{-/-} mice, but are closer to the innate cells than TCR $\gamma\delta^+$ T cells. Unexpectedly, however, TCR $\gamma\delta^-$ mice and CD1d^{-/-} mice developed pancreatitis after cerulein administration (Supplementary Figure 2). In addition, we eliminated the possibility that NK cells are involved in this model by showing that pre-administration of an anti-asialo GM1 monoclonal antibody did not affect the severity of the pancreatitis (Supplementary Figure 2). Overall, our data led to the conclusion that NK, NKT, and TCR $\gamma\delta^+$ T cells might not participate in the early stage of the pathogenesis of this model.

Therefore, it was interesting that the pancreatic CD11b^{high}CD11c⁻ population, which was absent under

steady-state conditions, emerged in cerulein-injected mice at the highest ratio among the immune cells in the damaged pancreas. The marked increase in this population at 8 hours after cerulein administration suggests that this population migrated from outside of the pancreas, rather than expanding within the pancreas from precursors. This notion was supported by the findings that the resident macrophages under steady-state conditions were in the Gr-1⁻ subpopulation (S1), whereas the migratory macrophages during the inflammation were in the Gr-1^{low} subpopulation (S2) (Figure 1). In addition, cerulein-administered RAG-2^{-/-} mice developed mild pancreatitis with a marked increase in the S2 macrophage subpopulation without the presence of T cells (Supplementary Figure 1).

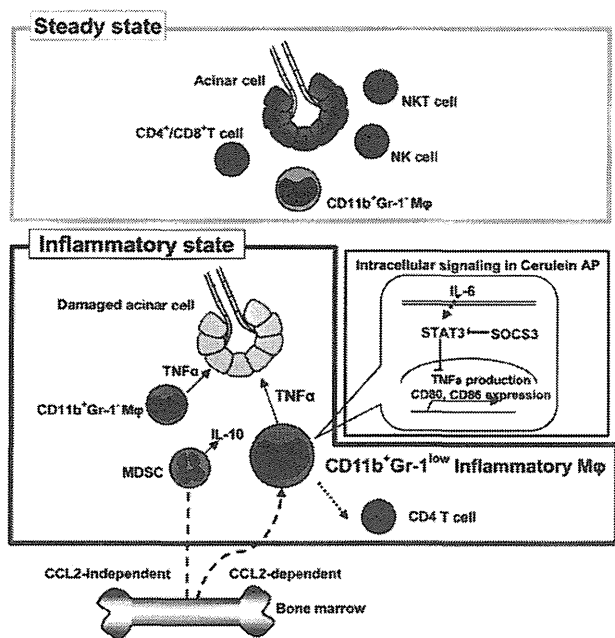


Figure 6. Two steps are required for development of cerulein-induced acute pancreatitis. Almost all sets of immune compartments, except for the CD11b^{high}CD11c⁻ population, reside in the pancreas under steady-state conditions (upper, green). During cerulein hyperstimulation (lower, red), the damaged acinar cells lead to CD11b^{high}Gr-1^{low} inflammatory macrophage migration into the pancreas in a CCL2-CCR2-dependent manner (step 1). Next, inflammatory macrophages are activated to produce TNF- α in a SOCS3-dependent manner (step 2). Finally, pancreatogenic CD4⁺ T cells interacted with the inflammatory macrophages establish the model. In contrast, granulocytes and IL-10-producing MDSCs migrate to the damaged pancreas in a CCL2-CCR2-independent manner.

In support of this, we detected up-regulation of CD80 and CD86 expression on pancreatic macrophages even in cerulein-administered RAG-2^{-/-} mice (Supplementary Figure 1), suggesting the involvement of innate immune cells at an early stage of this model. Despite speculation that interferon- γ produced by effector CD4⁺ T cells in the pancreas of cerulein-injected mice activates macrophages,²⁶ our results indicate that S2 and S3 macrophages/granulocytes/MDSCs are the initiators in this model, and acquired immune cells, particularly conventional CD4⁺ T cells, are the eventual effectors that establish the model, possibly through cross talk with activated macrophages/granulocytes and CD4⁺ T cells. The pancreas can be controlled by distinctive subpopulations of macrophages: resident CD11b^{high}Gr-1⁻ macrophages (S1) under steady-state conditions and migratory CD11b^{high}Gr-1^{low} macrophages (S2) during inflammation.

We further examined the characteristics of the CD11b^{high}Gr-1⁻ (S1), CD11b^{high}Gr-1^{low} (S2), and CD11b^{high}Gr-1^{high} (S3) subpopulations because it is possible that the S2 and S3 subpopulations can include granulocytes and/or MDSCs.¹⁸ We found that the S2 subpopulation that emerged during inflammation comprised morphologically and phenotypically homogeneous F4/80⁺CD11c⁻Ly6C^{high}Ly6G⁻ macrophages. These migratory cells should be responsible for development of

acute pancreatitis induced by cerulein injection, because they not only produced a huge amount of TNF- α , but were also significantly decreased in nondiseased CCL2^{-/-} mice injected with cerulein. In contrast, the S3 subpopulation did not express F4/80, and was composed of 2 subpopulations: dominant granulocyte-like cells with a segmented nucleus and minor macrophage-like cells with a horseshoe-shaped nucleus. Interestingly, the migration of the S3 subpopulation was not affected in nondiseased CCL2^{-/-} mice injected with cerulein, suggesting that the migration of S3 cells is not mediated by the CCR2/CCL2 axis. Furthermore, in sharp contrast to the TNF- α -expressing S2 subpopulation, approximately half of the S3 subpopulation expressed IL-10 but not TNF- α . Although we did not determine which S3 subpopulations produced IL-10 during inflammation of the pancreas, inflammatory TNF- α -expressing S2 cells and protective IL-10-expressing S3 cells (possibly MDSCs) may migrate to the damaged pancreas via a distinct migratory pathway.

Our parabiosis experiments led to the particularly important conclusion that pathological monocytes, which migrate to the pancreas and become activated TNF- α -producing macrophages, are not derived from constantly circulating monocytes, but from a certain reservoir of monocytes. The surprising finding was that when cerulein was injected into one parabiont and PBS was injected into the partner, only mice injected with cerulein developed pancreatitis. These findings indicate that intraperitoneally injected cerulein directly affected the pancreas only in the injected animal, and monocytes in a certain reservoir of only the diseased mice, which were not constantly circulating monocytes, were only recruited to the damaged pancreas, in which CCL2 expression is up-regulated,²¹ because the chimerism of macrophages in cerulein-injected mice should reach around 50% if constantly circulating mixed monocytes are recruited to the damaged pancreas. In this regard, we found that the absolute cell number of CD11b^{high}Gr-1^{low}Ly6C^{high} cells corresponding to the S2 population in the BM of mice injected with cerulein was significantly lower than that in PBS-injected mice, indicating that such cells are mobilized to the damaged pancreas from the BM.

After the migration of monocytes into the cerulein-induced damaged pancreas, the question arose as to which mechanisms of monocyte activation and differentiation to pathological macrophages operate in this model. To address this, we tested the possibility that SOCS3 plays a crucial role in the activation of pancreatic macrophages in this model. Consistent with this, it is known that both SOCS1 and SOCS3 participate in Toll-like receptor (TLR)/NF- κ B signaling in macrophages. Unlike the SOCS1 signaling pathway, SOCS3 is a key regulator that suppresses IL-6-mediated STAT3 activation. Because STAT3 activation results in suppression of TLR/NF- κ B signaling in macrophages, the lack of the SOCS3 signaling pathway can accelerate the STAT3 activation, resulting in the amelioration of pancreatitis in this model (Figure 6). Additional studies will be needed to determine which kinds of endogenous ligands stimulate

BASIC AND TRANSLATIONAL PANCREAS

TLR/NF- κ B signaling and activate SOCS3 in macrophages in the pathogenesis of acute pancreatitis.

Finally, we tested another model of acute pancreatitis, the L-Arg model, to determine a general concept for the pathogenesis of murine acute pancreatitis. We found not only that CD11b⁺CD11c⁻Gr-1^{low} S2 macrophages showed a marked increase in the inflamed pancreas of this second model, but also that CCL2^{-/-} mice were resistant to this model in accordance with the cerulein model. However, unlike the cerulein model, we did not detect statistically significant differences between L-Arg-injected WT mice and SOCS3cKO mice, suggesting that SOCS3 was not strongly involved in S2 macrophage activation in this model, although L-Arg-injected WT mice tended to develop mild pancreatitis. Therefore, CCL2/CCR2-dependent migratory macrophages are essential for the pathogenesis of acute pancreatitis, but the activation process of macrophages in the damaged pancreas occurs in a model-dependent manner.

In summary, the following consecutive immunological events are required for the development of cerulein-induced acute pancreatitis: CCL2/CCR2-dependent CD11b^{high}CD11c⁻Gr-1^{low}Ly6C^{high} monocyte/macrophage migration from the BM and SOCS3-dependent macrophage activation. These findings provide a new concept for therapeutic strategies against acute pancreatitis.

Supplementary Material

Note: To access the supplementary material accompanying this article, visit the online version of *Gastroenterology* at www.gastrojournal.org, and at doi: 10.1053/j.gastro.2008.07.064.

References

- Baron TH, Morgan DE. Acute necrotizing pancreatitis. *N Engl J Med* 1999;340:1412-1417.
- Sand J, Nordback I. Acute pancreatitis: risk of recurrence and late consequences of the disease. *Nat Rev Gastroenterol Hepatol* 2009;6:470-477.
- Saluja AK, Lerch MM, Phillips PA, et al. Why does pancreatic overstimulation cause pancreatitis? *Annu Rev Physiol* 2007;69:249-269.
- Hashimoto D, Ohmuraya M, Yamamura K, et al. Involvement of autophagy in trypsinogen activation within the pancreatic acinar cells. *J Cell Biol* 2008;181:1065-1072.
- Mareninova OA, Hermann K, Gukovskaya AS, et al. Impaired autophagic flux mediates acinar cell vacuole formation and trypsinogen activation in rodent models of acute pancreatitis. *J Clin Invest* 2009;119:3340-3355.
- Yang CY, Chang-Chien CS, Liaw YF. Controlled trial of protease inhibitor gabexate mesilate (FOY) in the treatment of acute pancreatitis. *Pancreas* 1987;2:698-700.
- Büchler M, Malfertheiner P, Beger HG, et al. Gabexate mesilate in human acute pancreatitis. German Pancreatitis Study Group. *Gastroenterology* 1993;104:1165-1170.
- Chen HM, Chen JC, Hwang TL, et al. Prospective and randomized study of gabexate mesilate for the treatment of severe acute pancreatitis with organ dysfunction. *Hepatogastroenterology* 2000;47:1147-1150.
- de Beaux AC, Palmer KR, Carter DC. Factors influencing morbidity and mortality in acute pancreatitis: an analysis of 279 cases. *Gut* 1995;37:121-126.
- Kylänpää ML, Repo H, Puolakkainen PA. Inflammation and immunosuppression in severe acute pancreatitis. *World J Gastroenterol* 2010;16:2867-2872.
- Sakai Y, Masamune A, Shimosegawa T, et al. Macrophage migration inhibitory factor is a critical mediator of severe acute pancreatitis. *Gastroenterology* 2003;124:725-736.
- Sandoval D, Gukovskaya A, Pandol SJ, et al. The role of neutrophils and platelet-activating factor in mediating experimental pancreatitis. *Gastroenterology*. 1996;111:1081-1091.
- Demols A, Le Moine O, Desalle F, et al. CD4⁺ T cells play an important role in acute experimental pancreatitis in mice. *Gastroenterology* 2000;118:582-590.
- Grady T, Liang P, Logsdon CD. Chemokine gene expression in rat pancreatic acinar cells is an early event associated with acute pancreatitis. *Gastroenterology* 1997;113:1966-1975.
- Pandol SJ, Saluja AK, Imrie CW, et al. Acute pancreatitis: bench to the bedside. *Gastroenterology* 2007;132:1127-1151.
- Chan YC, Leung PS. Acute pancreatitis: animal models and recent advances in basic research. *Pancreas* 2007;34:1-14.
- Domínguez PM, Ardavin C. Differentiation and function of mouse monocyte-derived dendritic cells in steady state and inflammation. *Immunol Rev* 2010;234:90-104.
- Gabrilovich DI, Nagaraj S. Myeloid-derived suppressor cells as regulators of the immune system. *Nat Rev Immunol* 2009;9:162-174.
- Serbina NV, Jia T, Hohl, et al. TM, Monocyte-mediated defense against microbial pathogens. *Annu Rev Immunol* 2008;26:421-452.
- Zhang Y, Rollins BJ. A dominant negative inhibitor indicates that monocyte chemoattractant protein 1 functions as a dimer. *Mol Cell Biol* 1995;15:4851-4855.
- Bhatia M, Ramnath RD, Chevali L, et al. Treatment with bindarit, a blocker of MCP-1 synthesis, protects mice against acute pancreatitis. *Am J Physiol Gastrointest Liver Physiol* 2005;288:1259-1265.
- Geissmann F, Manz MG, Jung S, et al. Development of monocytes, macrophages, and dendritic cells. *Science* 2010;327:656-661.
- Cuzzocrea S, Mazzon E, Thiemermann C, et al. Absence of endogenous interleukin-6 enhances the inflammatory response during acute pancreatitis induced by cerulein in mice. *Cytokine* 2002;18:274-285.
- Yoshimura A, Naka T, Kubo M. SOCS proteins, cytokine signaling and immune regulation. *Nat Rev Immunol* 2007;7:454-465.
- Hegyí P, Rakonczay Z Jr, Sári R, et al. L-arginine-induced experimental pancreatitis. *World J Gastroenterol* 2004;10:2003-2009.
- Hayashi T, Ishida Y, Kimura A, et al. IFN-gamma protects cerulein-induced acute pancreatitis by repressing NF-kappa B activation. *J Immunol* 2007;178:7385-7394.

Received November 25, 2010. Accepted December 9, 2011.

Reprint requests

Address requests for reprints to: Toshifumi Hibi, MD, PhD, Division of Gastroenterology and Hepatology, Department of Internal Medicine, Keio University School of Medicine, Tokyo 180-8582, Japan. e-mail: thibi@sc.itc.keio.ac.jp; Fax: +81-3-3341-3631.

Conflicts of interest

The authors disclose no conflicts.

Funding

This study was supported in part by Grants-in-Aid for Scientific Research, Scientific Research on Priority Areas, Exploratory Research and Creative Scientific Research from the Japanese Ministry of Education, Culture, Sports, Science and Technology; by the Research Fund of Yakult Medical Foundation; and by the Keio University Medical Fund.

Supplementary Materials and Methods

Mice

C57BL/6 mice were purchased from Japan CLEA (Tokyo, Japan). C57BL/6-Ly5.1 and C57BL/6-RAG-2^{-/-} mice were obtained from Taconic Laboratory (Hudson, NY) and Central Laboratories for Experimental Animals (Kawasaki, Japan). Macrophage chemoattractant protein 1 knockout (MCP-1^{-/-} [also known as CCL2^{-/-}]) mice¹ and LTA^{-/-} mice² were purchased from Jackson Laboratories (Bar Harbor, ME). Interleukin-23 p19 knockout (IL-23p19^{-/-}) mice,³ $\gamma\delta$ T cell receptor knockout (TCR $\gamma\delta$ ^{-/-}) mice,⁴ lysozyme M (LysM)-Cre/Socs1^{fllox/fllox} conditional knockout (cKO) mice, and LysM-Cre/Socs3^{fllox/fllox} cKO mice were previously generated by one of the authors (A. Yoshimura).⁵ CD1d^{-/-} mice were previously generated by S.K. Mendiratta.⁶ All mice had the C57BL/6 background and were housed in our specific pathogen-free animal facility. All experiments were approved by the regional animal study committees and performed according to the guidelines of the animal ethics committee of Keio University, Tokyo, Japan.

Induction of Acute Pancreatitis

Cerulein (Sigma-Aldrich, St. Louis, MO) was dissolved with phosphate-buffered saline (PBS) (Wako, Osaka, Japan) and administered intraperitoneally at a dose of 50 μ g/kg at intervals of 1 h (total of 8 injections). In some experiments using parabionts (Figure 3, Group 3), cerulein was administered unilaterally at a dose of 100 μ g/kg. The mice were euthanized by cervical dislocation at 1 h after the last cerulein injection. Before euthanasia, whole blood was collected from the ocular artery under light ether anesthesia. After euthanasia, the pancreas and spleen were excised and immediately weighed. For histological analysis, the pancreas was fixed in 10% formaldehyde (Wako) for H&E staining. For L-Arginine-induced Acute Pancreatitis, L-Arginine monohydrochloride (Sigma-Aldrich) was dissolved in saline and administered intraperitoneally in two doses of 4 g/kg spaced 1 h apart and mice were euthanized at 72 h later as previously described.⁷

Histological Score

Microscopic images were taken under a light microscope (Nikon, Tokyo, Japan) using ACT software (Nikon). Histological scoring was performed using a point-counting morphometry method as described previously.⁸ Briefly, a 10 \times 10- μ m grid was superimposed on three randomly-chosen microscopic images of every section, and the interstitial space under each grid point was counted.

Serum Amylase and Lipase Levels

Sera were diluted 5-fold with pure water and stored at -80°C until analysis. The amylase and lipase levels were analyzed according to standard procedures.

Mononuclear Cell Isolation

For mononuclear cell isolation, the pancreas was minced and digested with 3 mg/ml collagenase A (Roche, Mannheim, Germany) for 15 min. The digest was filtered through a 40- μ m cell strainer and washed with 1.5% FCS-containing Hank's balanced salt solution. Next, the suspended cells were centrifuged at 50 \times g for 30 s to eliminate the major debris. The total mononuclear cells were further purified by 40–70% Percoll gradient centrifugation. Splenic mononuclear cells were isolated by mechanical homogenization. Bone marrow cells were isolated from the femur.

Flow Cytometry Analysis

Isolated cells were incubated with an anti-CD16/CD32 antibody (BD Pharmingen, Tokyo, Japan) to prevent non-specific antibody binding.⁹ Surface antigens were stained with the following antibodies conjugated with fluorescein isothiocyanate (FITC), phycoerythrin (PE), allophycocyanin (APC), phycoerythrin-Cy7 (PECy7), or allophycocyanin-Cy7 (APCCy7): CD3e-FITC, CD3e-APCCy7, CD4-PE, CD4-PECy7, CD8 α -APCCy7, NK1.1-APC, $\gamma\delta$ TCR-FITC, CD11b-PECy7, CD11c-APC, Ly6G and Ly6C-APCCy7 (Gr-1, clone: RB6-8C5), Ly6G-PE (clone: 1A8), Ly5.2-FITC, CD49b-FITC (clone: DX5), CD80-PE, CD86-PE, Ly6C-FITC, and B220-FITC. The corresponding isotype IgGs were obtained from BD Pharmingen. F4/80-APC was obtained from eBioscience. Dead cells were eliminated by 7-AAD (BD Pharmingen) according to the manufacturer's protocol. Flow cytometry was performed with a FACSCanto II and cell sorting was performed with a FACSARIA (both from BD Biosciences, San Jose, CA). All data were re-analyzed with FlowJo Version 7.2.5 software (TreeStar, Ashland, OR). The mean fluorescence intensity (MFI) was calculated as follows: MFI = (CD80 or CD86 geometric mean) - (isotype geometric mean).

Cell Counts

Isolated cells were counted under a light microscope. To avoid counting dead cells, cells were incubated with Gibco Trypan Blue Stain 0.4% (Invitrogen, Carlsbad, CA). The absolute cell number of mononuclear cells in the pancreas was estimated as follows: Total cell count = (isolated cell count) \times (total wet weight)/(wet weight used for cell isolation). The cell number in each leukocyte subset was calculated by regarding the 7-AAD⁻/characteristic FSC, SSC-gated monocyte subset as counted cells.

Parabiosis

Surgical gloves and autoclaved sterilized instruments were used. Sodium pentobarbital was administered intraperitoneally for sedation. After shaving the corresponding lateral aspects of each mouse, matching skin incisions were made from the base of the anterior to posterior extremities of each mouse, and the subcutane-

ous fascia was bluntly dissected to create about 1/2 cm of free skin. The parabionts were then combined by suturing the corresponding free skin densely with surgical clips.¹⁰ The percent chimerism was defined for gated monocytes as % CD45.1⁺ cells/Ly5.1⁺ + Ly5.2⁺ cells in Ly5.2 mice and as % Ly5.2 cells/Ly5.1⁺ + Ly5.2⁻ cells in Ly5.1 mice in the indicated cells. In some experiments, parabiosis surgery was performed between Ly5.1⁺ WT and Ly5.2⁺ CCL2^{-/-} mice, and both mice were injected with cerulein (50 µg/kg for each mouse) at 2 wk after the surgery (Supplementary Figure 6A).

Intracellular Cytokine Staining

Isolated cells were cultured with or without 1 µg/ml of lipopolysaccharide (LPS) in 10% FCS-containing RPMI1640 medium for 5 h. After surface staining with CD11b-PECy7, Ly6G and Ly6C-APCCy7, and CD3e-PerCPCy5.5 antibodies, the cells were fixed and permeabilized with a Cytotfix/Cytoperm Kit (BD Biosciences) according to the manufacturer's protocol. For cytokine staining, IL-10-APC and TNFα-PE antibodies (BD Pharmingen) were used.

Phosphorylation of Transcription Factors

Total collagenase-digested cells were harvested for phosphorylation analyses of p38 MAPK and STAT3 using the phosflow method (BD Pharmingen) according to the manufacturer's instructions. For flow cytometry staining, F4/80-FITC, STAT3 (pY705)-PE, and p38MAPK-PE antibodies (BD Pharmingen) were used.

NK Cell Depletion

Selective depletion of NK cells was achieved with a rabbit anti-asialoGM1 monoclonal antibody (250 µg intraperitoneal; Wako) at 24 h and 72 h before the first cerulein injection. Control mice were injected with non-specific IgG (Sigma-Aldrich) using the same regimen. Pancreatic and splenic NK cell depletion was confirmed by flow cytometry (data not shown).

Acinar Cell Isolation and Cytotoxicity Assay

Acinar cells were isolated from the normal pancreas as previously described with some modifications.¹² Briefly, collagenase A solution (0.18 mg/ml) was injected into the pancreas and thereafter the tissue was digested for 30 min. The digest tissue was further broken up to single acinar cells or acini by pipetting and washed with 4% BSA-containing RPMI1640 medium. The viability was confirmed >95% and the purity was >99% by flow cytometry with the staining of 7-AAD and anti-CD45.2 Ab. Acinar cells were cultured in 10%FCS-containing RPMI1640 for 5 h with or without FACSaria-sorted S2 macrophages, S3 granulocytes, and a hamster anti-mouse TNF-α antibody (clone: TN3-19.12; BioLegend, San Diego, CA) on 48-well plates. Apoptotic and dead acinar cells were evaluated by flow cytometry after staining with

annexin V (BD Pharmingen) and 7-AAD according to the manufacturer's protocol.

Cytokine Bead Assay

Cytokine bead assays were performed using a mouse Th1/Th2/Th17 CBA Kit (BD Biosciences) according to the manufacturer's protocol.

Macrophage Depletion

Macrophages were depleted by intraperitoneal injection of Clodronate Liposomes (50 mg/kg; Encapsula Nanosciences, Nashville, TN) at 24 h before the first injection of cerulein. For control mice, Plain Liposomes (Encapsula Nanosciences) were injected. Macrophage depletion was confirmed by flow cytometry of splenic macrophages (data not shown).

Quantitative RT-PCR

Total RNA was extracted from FACSaria-sorted CD11b⁺ macrophages using the TRIzol reagent (Invitrogen) according to the manufacturer's protocol. SOCS1 (Mm00782550_s1) and SOCS3 (Mm00545913_s1) mRNA expression was assessed by real-time PCR using a TaqMan Gene Expression Assays Kit (Applied Biosystems, Foster City, CA) according to the manufacturer's protocol. Briefly, 1 µg of total RNA was reverse-transcribed to cDNA using TaqMan Universal Master Mix and quantitative PCR was performed using a StepOnePlusTM System (Applied Biosystems) and TaqMan technology. Data were analyzed using the DCT method, and the expression levels were normalized by the expression of b-actin as an internal control.

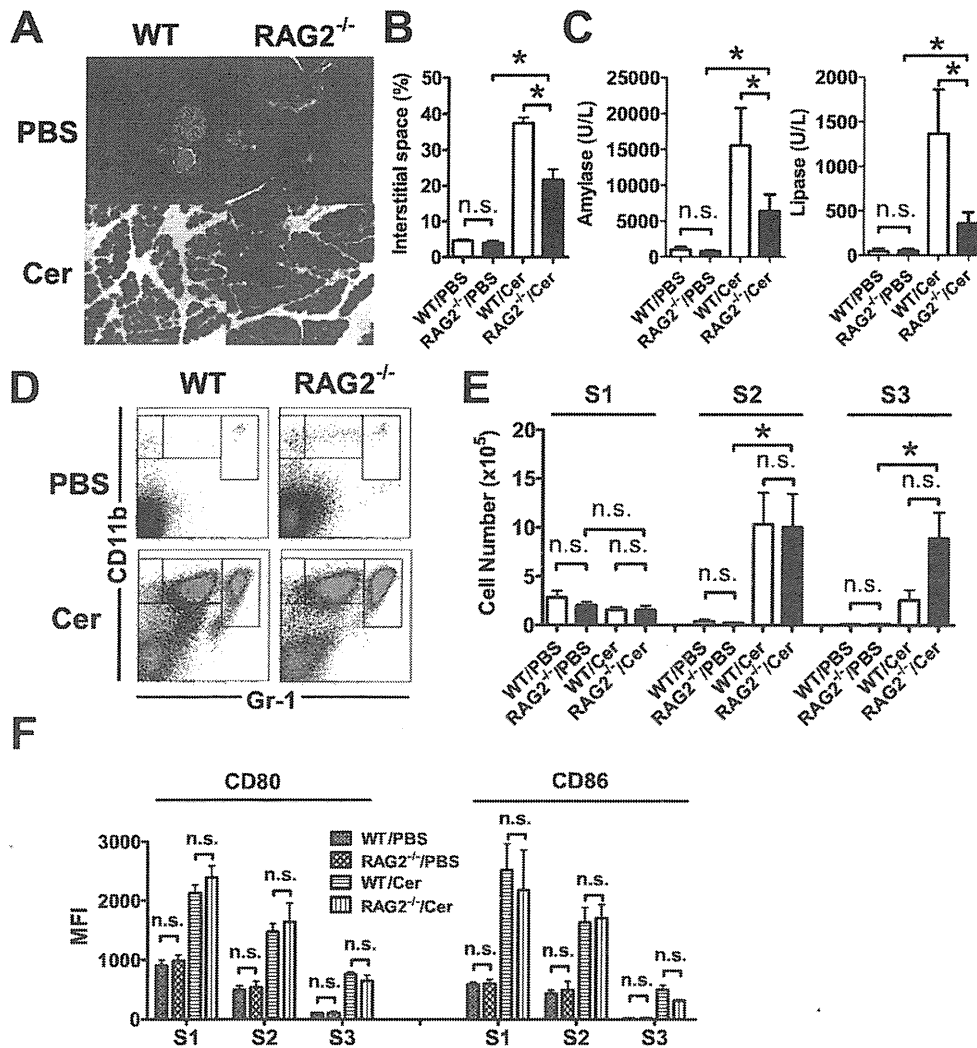
Statistical Analysis

The Mann-Whitney U test was used for statistical analysis of the histological scores, and an unpaired Student's *t* test was used for other analyses. All analyses were performed with JMP software version 7.0 (SAS Institute Inc., Cary, NC), and values of *P* < 0.05 were considered to indicate statistical significance. All graphs were drawn using GraphPad Prism 5 for Windows software (GraphPad Software Inc., San Diego, CA), and all data were presented as means ± SEM.

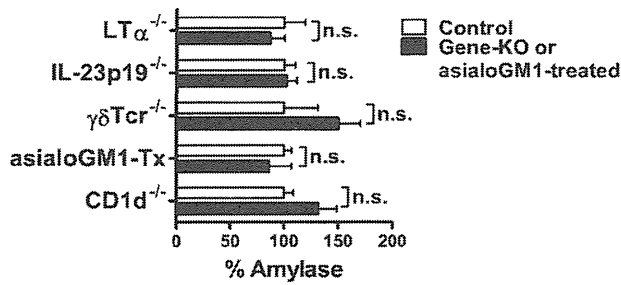
Supplemental References

1. Lu B, Rutledge BJ, Gu L, et al. Abnormalities in monocyte recruitment and cytokine expression in monocyte chemoattractant protein 1-deficient mice. *J Exp Med*. 1998;187:601-8.
2. De Togni P, Joellner NH, Ruddle, et al. Abnormal development of peripheral lymphoid organs in mice deficient in Lymphotoxin. *Science*. 1994;264:703-707.
3. Cua DJ, Sherlock J, Chen Y, et al. Interleukin-23 rather than interleukin-12 is the critical cytokine for autoimmune inflammation of the brain. *Nature*. 2003; 421: 744-748.
4. Shichita T, Sugiyama Y, Ooboshi H, et al. Pivotal role of cerebral interleukin-17-producing gammadeltaT cells in the delayed phase of ischemic brain injury. *Nat Med* 2009;15:946-50.

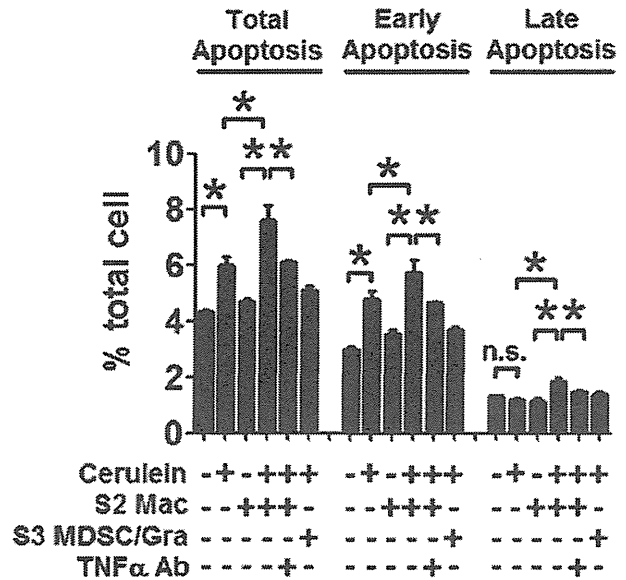
5. Yasukawa H, Ohishi M, Mori H, et al. IL-6 induces an anti-inflammatory response in the absence of SOCS3 in macrophages. *Nat Immunol* 2003;4:551–6.
6. Mendiratta SK, Martin WD, Hong S, et al. CD1d1 mutant mice are deficient in natural T cells that promptly produce IL-4. *Immunity*. 1997;6:469–477.
7. Dawra R, Sharif R, Saluja AK, et al. Development of a new mouse model of acute pancreatitis induced by administration of L-arginine. *Am J Physiol Gastrointest Liver Physiol*. 2007;292:1009–18.
8. Barreto SG, Carati CJ, Saccone GT, et al. The combination of neurokinin-1 and galanin receptor antagonists ameliorates cerulein-induced acute pancreatitis in mice. *Peptides*. 2010;31:315–321.
9. Mikami Y, Kanai T, Sujino T, et al. Competition between colitogenic Th1 and Th17 cells contributes to the amelioration of colitis. *Eur J Immunol* 2010;40:2409–22.
10. Tomita T, Kanai T, Nemoto Y, et al. Systemic, but not intestinal, IL-7 is essential for the persistence of chronic colitis. *J Immunol* 2008; 180: 383–90.
11. Nakamura Y, Do JH, Pandolfi SJ, et al. Inflammatory cells regulate p53 and caspases in acute pancreatitis. *Am J Physiol Gastrointest Liver Physiol*. 2010;298:92–100.



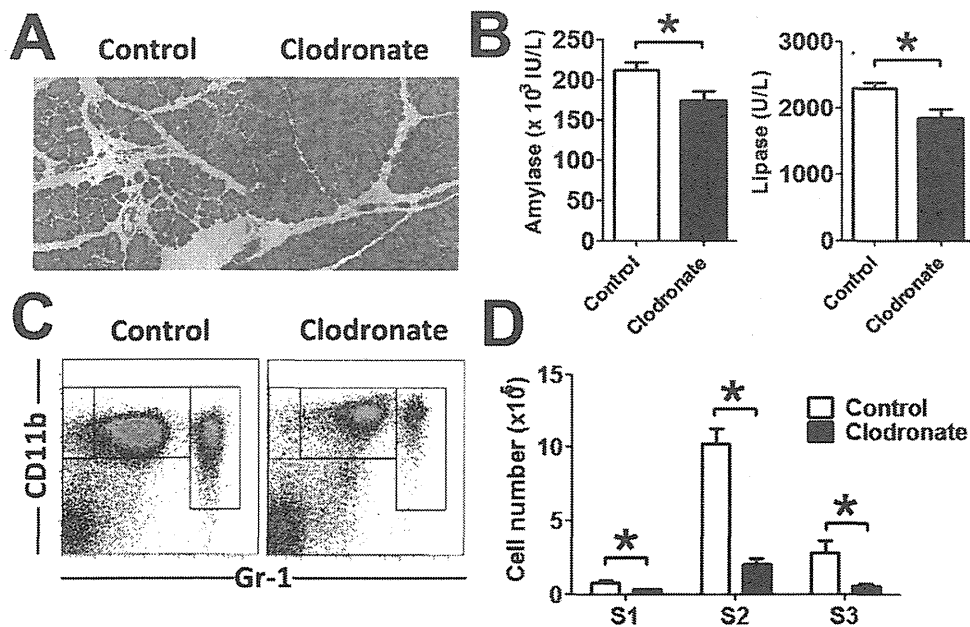
Supplementary Figure 1. Cerulein-administered RAG2^{-/-} mice develop mild pancreatitis. (A) H&E staining of the pancreas of cerulein- or PBS-administered WT or RAG2^{-/-} mice. Original magnification, ×200. (B) Histological scores (n = 6). *P < .05; n.s., not significant. (C) Serum amylase and lipase levels (n = 10). *P < .05; n.s., not significant. (D) Expression of CD11b/Gr-1 on pancreatic cells of the indicated mice administered cerulein. (E) Absolute cell numbers of each subpopulation (n = 4) of the indicated mice administered cerulein or PBS. *P < .05; n.s., not significant. (F) Mean fluorescence intensities of CD80 and CD86 on each subpopulation (n = 4) of the indicated mice administered cerulein or PBS. Data are representative of two independent experiments. n.s., not significant. Cer; cerulein.



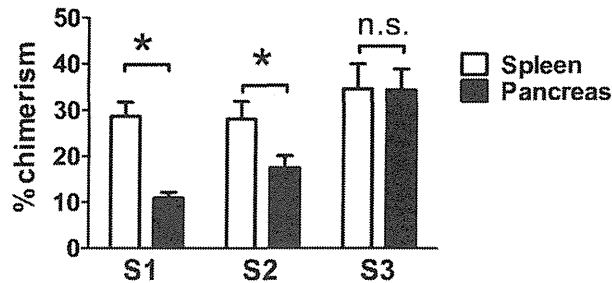
Supplementary Figure 2. Induction of pancreatitis by cerulein administration in various gene-deficient mice and anti-asialoGM1 monoclonal antibody-treated mice. LTα^{-/-} mice and littermate controls (*n* = 5 each), IL-23p19^{-/-} mice and littermate controls (*n* = 13 each), CD1d^{-/-} mice and littermate controls (*n* = 7 each), γδTcr^{-/-} mice and littermate controls (*n* = 4 each), and anti-asialoGM1 mAb- or isotype-matched monoclonal antibody-treated mice (*n* = 5 each) were administered cerulein at intervals of 1 h (total of 8 injections). The serum amylase levels were measured and %amylase was calculated as follows: (serum amylase level of each individual)/(mean amylase level of control).



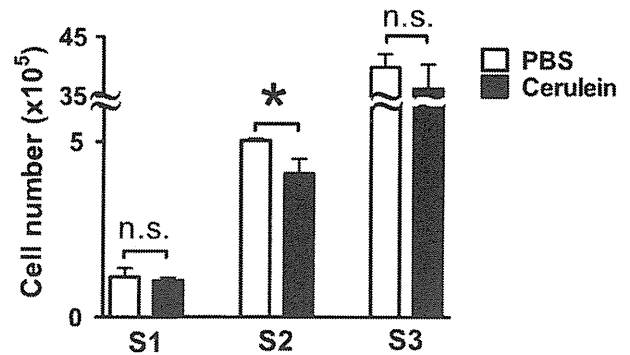
Supplementary Figure 4. S2 macrophage-derived TNF-α regulates acinar cell apoptosis. Acinar cells were cultured for 5 h with or without 10 nM cerulein, with or without 1 × 10⁵ S2 macrophages or S3 granulocytes (Gra)/MDSCs, and with or without 1 μg of an anti-TNF-α antibody. The viability of the cultured acinar cells was evaluated by flow cytometry after annexin V/7-AAD staining. Early apoptosis was defined as the annexin V⁺/7-AAD⁻ subpopulation and late apoptosis was defined as the annexin V⁺/7-AAD⁺ subpopulation of the total cells (*n* = 6/each group).



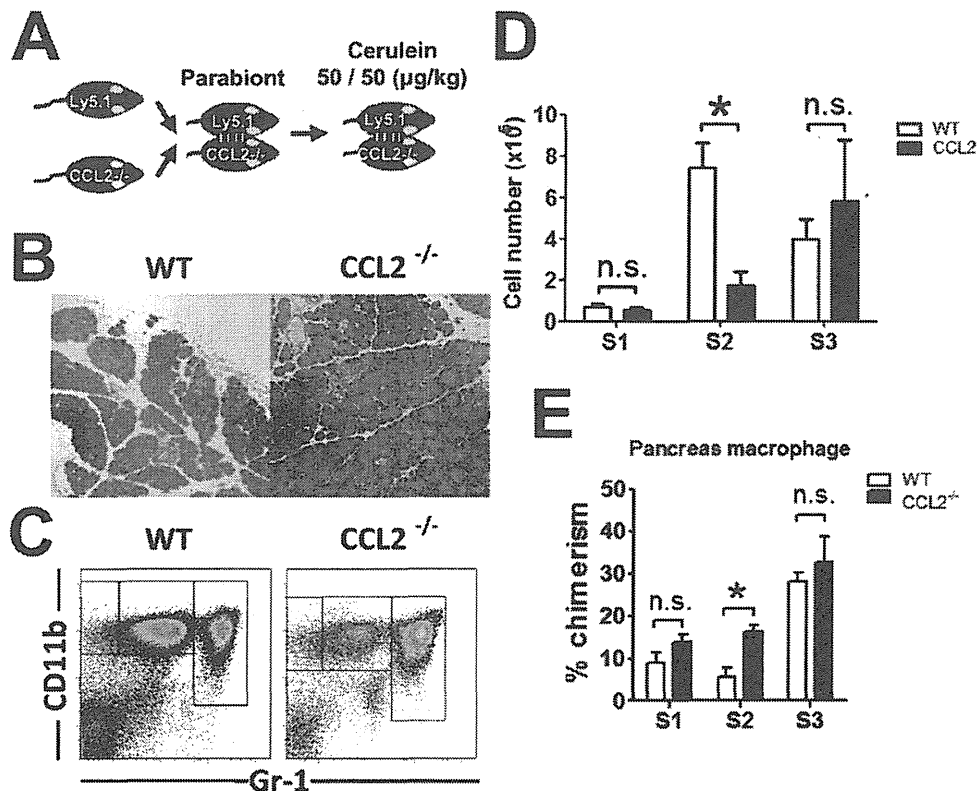
Supplementary Figure 3. Macrophage depletion reduces the severity of cerulein-induced acute pancreatitis. Macrophages were depleted by injection of Clodronate Liposomes at 24 h before cerulein administration. (A) H&E staining of the pancreas of the indicated cerulein-administered mice. Original magnification, ×200. (B) Serum amylase and lipase levels (*n* = 5). **P* < .05; n.s., not significant. (C) Expression of CD11b/Gr-1 on pancreatic cells of the indicated mice administered cerulein. (D) Absolute cell numbers of each subpopulation (*n* = 5) of the indicated mice. Data are representative of two independent experiments. **P* < .05.



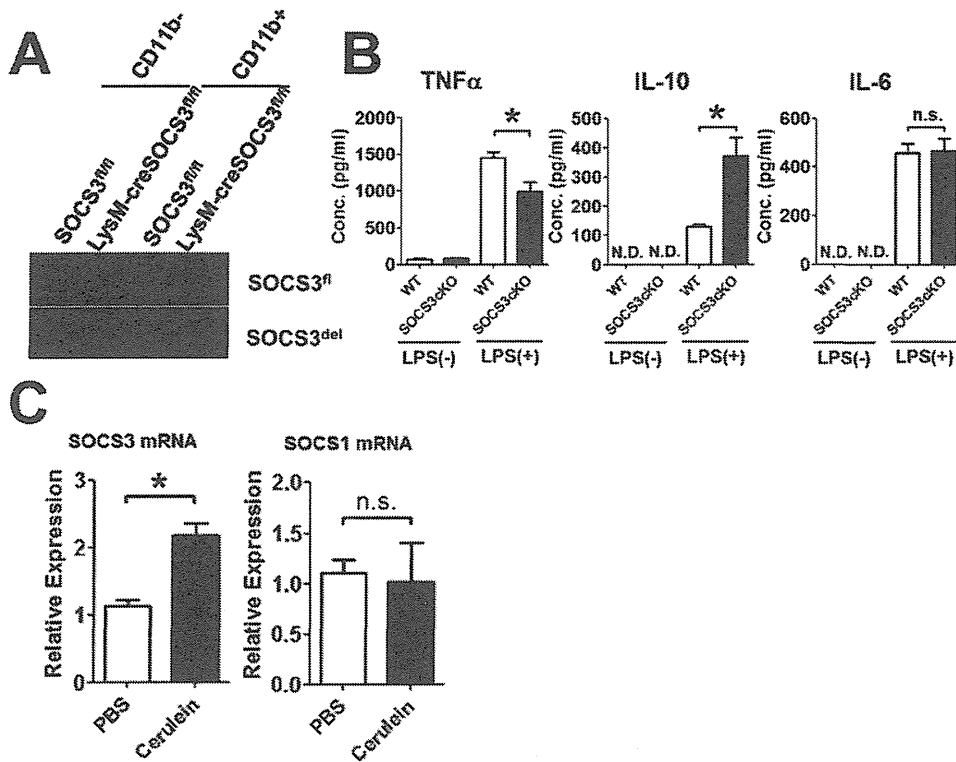
Supplementary Figure 5. Hemodynamics of pancreatic mononuclear cells. Parabiosis surgery was performed as depicted in Figure 4A. The percentages of chimerism of the pancreatic and splenic S1, S2, and S3 subpopulations were determined by using non-treated parabionts at 5 wk after the operation ($n = 4$).



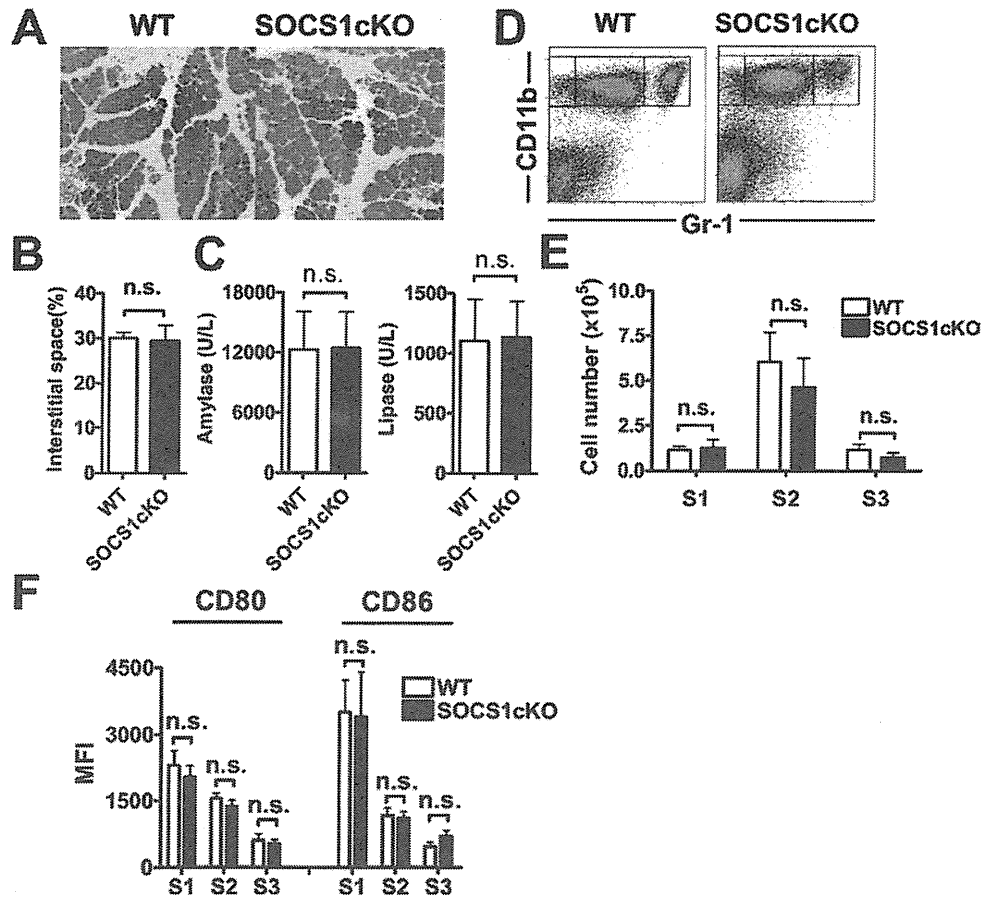
Supplementary Figure 7. BM is a reservoir for CD11b^{high}Gr-1^{low}Ly6C^{high} S2 macrophages in the development of cerulein-induced pancreatitis. The absolute cell numbers of each BM cell subpopulation in cerulein- or PBS-administered mice ($n = 4$) are shown. Each mouse was injected intraperitoneally at intervals of 1 h (total of 8 injections), and euthanized at 1 h after the last injection. * $P < .05$; n.s., not significant.



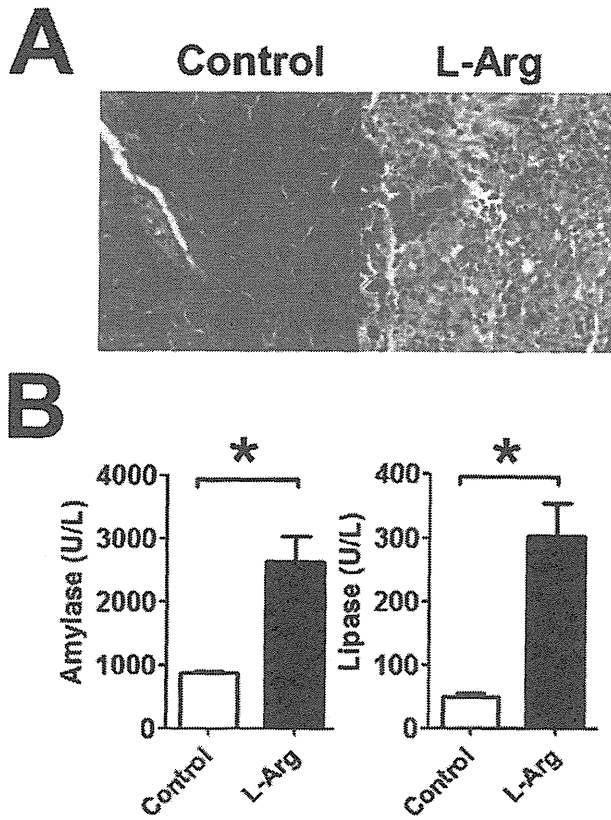
Supplementary Figure 6. Pancreatic S2 macrophages are recruited from the host reservoir in both WT and CCL2^{-/-} mice. (A) Study design. Parabionts of Ly5.1-WT mice combined with Ly5.2-CCL2^{-/-} mice were administered 50 μ g/kg of cerulein bilaterally at 2 wk after the operation. (B) H&E staining of the pancreas. Original magnification, $\times 200$. (C) Flow cytometry of CD11b/Gr-1 and (D) absolute cell numbers of each subpopulation ($n = 4$). * $P < 0.05$; n.s., not significant. (E) Percentages of chimerism of each subpopulation ($n = 4$). * $P < .05$; n.s., not significant.



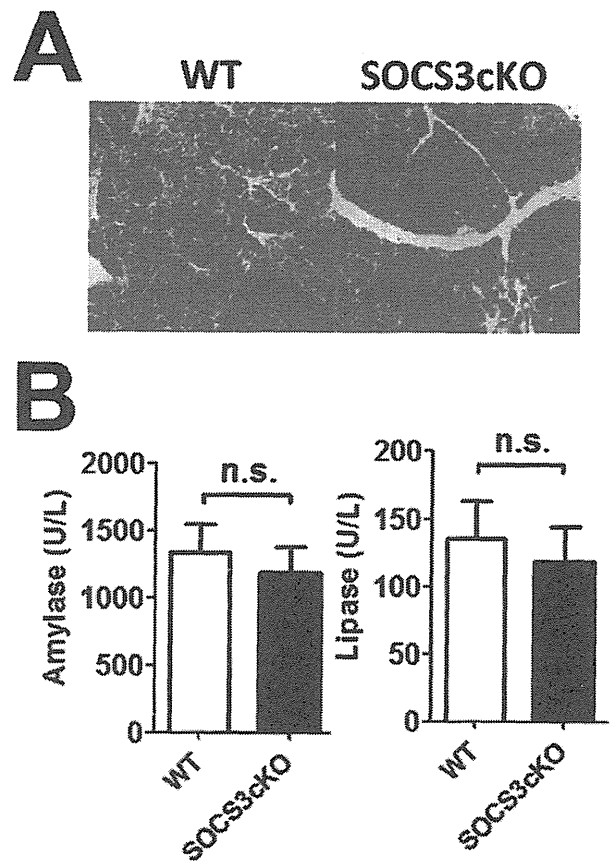
Supplementary Figure 8. SOCS3 is upregulated during cerulein-induced acute pancreatitis. (A) SOCS3 is deleted in CD11b⁺ pancreatic macrophages. Data are representative of three independent experiments. (B) LPS-mediated secretion of proinflammatory cytokines in splenic CD11b⁺ macrophages (*n* = 4). In the presence of 1 μ g/ml LPS, 1×10^5 splenic WT or SOCS3-deficient CD11b⁺ macrophages were cultured for 24 h with 10% FCS-containing RPMI1640 medium on 96-well round-bottom plates. Cytokine secretion was analyzed by cytokine bead assays. (C) SOCS3, but not SOCS1, mRNA is upregulated in pancreatic CD11b⁺ macrophages during cerulein-induced acute pancreatitis (*n* = 3). Data are representative of two independent experiments.



Supplementary Figure 9. SOCS1 in macrophages does not affect the severity of cerulein-induced pancreatitis. (A) H&E staining of the pancreas in cerulein-administered mice. Original magnification, $\times 200$. (B) Histological scores ($n = 3$). (C) Serum amylase and lipase levels ($n = 3$). (D) Expression of CD11b/Gr-1. (E) Absolute cell numbers of each pancreatic subpopulation ($n = 3$). n.s., not significant. (F) Mean fluorescence intensities of CD80 and CD86 on pancreatic cells ($n = 3$). n.s., not significant.



Supplementary Figure 10. L-Arginine-induced acute pancreatitis. Acute pancreatitis was induced by two sequential administrations of L-Arginine. (A) H&E staining of the pancreas of L-Arginine- or saline-administered mice. Original magnification, $\times 200$. (B) Serum amylase and lipase levels ($n = 4$). * $P < .05$. Data are representative of four independent experiments. L-Arg; L-Arginine.



Supplementary Figure 11. SOCS3 in macrophages does not regulate the severity of L-Arginine-induced acute pancreatitis. (A) H&E staining of the pancreas in L-Arginine-administered mice. Original magnification, $\times 200$. (B) Serum amylase and lipase levels ($n = 17$). Data were pooled from three independent experiments. n.s., not significant.

Altered Oligosaccharide Structures Reduce Colitis Induction in Mice Defective in β -1,4-Galactosyltransferase

SHINICHIRO SHINZAKI,^{*,†} HIDEKI IJIMA,^{*} HIRONOBU FUJII,[‡] ERI KUROKI,[‡] NORIKA TATSUNAKA,[‡] TAKAHIRO INOUE,^{*} SACHIKO NAKAJIMA,^{*} SATOSHI EGAWA,^{*} TATSUYA KANTO,^{*,§} MASAHIKO TSUJII,^{*} EIICHI MORII,^{||} SHUNSAKU TAKEISHI,^{||} MASAHIDE ASANO,[#] TETSUO TAKEHARA,^{*} NORIO HAYASHI,^{*} and EIJI MIYOSHI[†]

^{*}Departments of Gastroenterology and Hepatology, [†]Molecular Biochemistry and Clinical Investigation, [‡]Dendritic Cell Biology and Clinical Application, and

[§]Pathology, Osaka University Graduate School of Medicine, Osaka; ^{||}GP BioScience Ltd, Yokohama; and the [#]Division of Transgenic Animal Science, Kanazawa University Advanced Science Research Center, Kanazawa, Japan

BACKGROUND & AIMS: Oligosaccharide modifications induce various functional changes in immune cells. The galactose-deficient fraction of fucosylated IgG oligosaccharides is increased, whereas that of β -1,4-galactosyltransferase I (B4GalTI) is reduced, in patients with Crohn's disease. We investigated the role of oligosaccharide modification in the pathophysiology of colitis using *B4galt1*-deficient mice. **METHODS:** Colitis severity was compared between *B4galt1*^{+/-} and *B4galt1*^{+/+} mice. B cells isolated from *B4galt1*^{+/-} and *B4galt1*^{+/+} mice were adoptively transferred to recombination activating gene 2^{-/-} mice, in which colitis was induced by administration of CD4⁺CD62L⁺ T cells. Cell-surface glycan profiles were determined by lectin microarray analysis. Cytokine production was determined in a coculture of various types of cells isolated from either *B4galt1*^{+/-} or *B4galt1*^{+/+} mice. **RESULTS:** Colitis induction by dextran sodium sulfate or trinitrobenzene sulfonic acid was significantly reduced in *B4galt1*^{+/-} mice, which had galactose deficiency in IgG oligosaccharides (similar to patients with Crohn's disease) compared with *B4galt1*^{+/+} mice. Amelioration of colitis was associated with increased production of interleukin-10 by macrophages in *B4galt1*^{+/-} mice. Colitis induction in recombination activating gene 2^{-/-} mice by administration of CD4⁺CD62L⁺ T cells was reduced by cotransfer of B cells isolated from *B4galt1*^{+/-}, but not from *B4galt1*^{+/+} mice. Lectin microarray analysis revealed increased expression of polylectosamines on *B4galt1*^{+/-} B cells and macrophages, compared with *B4galt1*^{+/+} cells. The production of interleukin-10 from macrophages was induced via their direct interaction with *B4galt1*^{+/-} B cells. **CONCLUSIONS:** Altered oligosaccharide structures on immune cells modulate mucosal inflammation. Oligosaccharides in immune cells might be a therapeutic target for inflammatory bowel diseases.

Keywords: IBD; Mouse Model; Immune Regulation; CD.

Inflammatory bowel disease (IBD), including Crohn's disease (CD) and ulcerative colitis, is characterized as a chronic relapsing and remitting process in the digestive tract. Although the precise etiology of IBD remains unknown, both genetic susceptibility and dysregulation of mucosal immune responses against enteric host flora have

pivotal roles in its pathogenesis.¹ We recently demonstrated that oligosaccharide structures in serum IgG are dynamically changed in patients with IBD compared with healthy subjects.² IgG carries *N*-linked oligosaccharides at the C γ 2 domain of the Fc fragment at asparagine 297.^{3,4} The proportion of the agalactosyl fraction in the fucosylated oligosaccharides of human IgG is significantly higher in patients with CD than in patients with ulcerative colitis or in healthy volunteers.² In addition, agalactosyl IgG levels correlate with disease activity and the clinical course of CD.² These findings suggest that changes in the IgG oligosaccharide structure relate to the pathogenesis of CD. β -1,4-galactosyltransferase I (B4GalTI) conjugates galactose to the outer arm of *N*-acetylglucosamine in *N*-linked oligosaccharides of IgG and B4GalTI levels are associated with extension of the terminal galactose in IgG.⁵ In fact, B4GalTI activity and messenger RNA expression in B cells or plasma cells are lower in CD than in ulcerative colitis or disease controls.² The roles of oligosaccharide alterations in CD, however, have not yet been investigated.

Recent reports demonstrate that B cells and immunoglobulins have protective roles in IBD. Mizoguchi et al reported that B cells in mesenteric lymph nodes (MLN) containing the regulatory B-cell subset protects against colitis in murine colitis models.⁶ Intravenous immunoglobulin therapy is also effective for the treatment of human IBD.⁷ Although immunoglobulins and B cells have protective roles in IBD, it is not known whether oligosaccharide alterations via B4GalTI deficiency affect immune function in CD.

In the present study, we explored the pathophysiologic role of agalactosyl oligosaccharide alterations in IBD using murine colitis models. We found that *B4galt1*^{+/-} mice, which exhibit decreased B4GalTI activity, were protected against murine colitis models compared with wild-type mice with up-regulation of interleukin (IL)-10 production

Abbreviations used in this paper: B4GalTI, β -1,4-galactosyltransferase I; CD, Crohn's disease; DSA, *Datura stramonium* agglutinin; DSS, dextran sodium sulfate; IBD, inflammatory bowel disease; IFN, interferon; IL, interleukin; LP, lamina propria; LPS, lipopolysaccharides; MLN, mesenteric lymph nodes; PE, phycoerythrin; Rag, recombination activating gene; SP, spleen; TNBS, trinitrobenzene sulfonic acid.

© 2012 by the AGA Institute

0016-5085/\$36.00

doi:10.1053/j.gastro.2012.02.008

from macrophages. The mechanisms for the enhanced production of IL-10 due to the alteration of oligosaccharides were further evaluated.

Materials and Methods

Mice

B4galt1^{+/-} mice (C57BL/6 background) were generated as described previously.⁸ *Il-10*^{-/-} mice (C57BL/6 background) were purchased from the Jackson Laboratory (Bar Harbor, ME). C57BL/6 mice and recombination activating gene (*Rag*) 2^{-/-} mice were purchased from Japan Clea (Tokyo, Japan) and Taconic Inc. (Hudson, NY), respectively. All mice were kept under specific pathogen-free conditions in an environmentally controlled clean room at the Institute of Experimental Animal Sciences, Osaka University Graduate School of Medicine. The Institutional Committee on Animal Research approved the experiments.

Induction of Colitis

To generate dextran sodium sulfate (DSS)-induced colitis, mice were provided with 3% DSS (molecular weight 35,000–50,000 Da; MP Biomedicals, Solon, OH) in the drinking water ad libitum for 7 days. After administration of normal water for the following 3 days, the mice were killed on day 10. Trinitrobenzene sulfonic acid (TNBS)-induced colitis was generated as described previously.⁹ To generate colitis by adoptive transfer, CD4⁺CD62L⁺ naive T cells were transferred to immunodeficient *Rag2*^{-/-} mice as described previously.¹⁰ Briefly, splenic CD4⁺CD62L⁺ cells isolated from female C57BL/6 mice using a mouse CD4 naive T-cell column kit (R&D Systems, Minneapolis, MN) were intraperitoneally injected into *Rag2*^{-/-} mice (5×10^5 cells/mouse). Mice were killed at 10 weeks after transfer. In some experiments, CD19⁺ B cells were isolated from the MLN of *B4galt1*^{+/-} or *B4galt1*^{+/+} mice with CD19 magnetic beads (Miltenyi Biotech, Bergisch Gladbach, Germany), and 5×10^5 cells were intraperitoneally injected into *Rag2*^{-/-} mice.

Serum IgG Oligosaccharide Analysis

IgG purification from the sera of mice and subsequent IgG oligosaccharide analysis were performed as described previously.² Briefly, serum IgG was purified using protein G sepharose and N-linked oligosaccharides were released from serum IgG, labeled with 2-aminopyridine, and analyzed on a reversed phase high-performance liquid chromatography system (Waters Corp., Milford, MA).

Histologic Analysis

Formalin-fixed tissue samples were paraffin-embedded and proximal/distal colon sections were analyzed by H&E staining. Histologic scores were determined using individual scores for DSS colitis,¹¹ TNBS colitis,⁹ IL-10-deficient colitis,¹² and CD4⁺CD62L⁺ adoptive-transferred colitis.¹³ Histology was examined by a well-trained pathologist (E.M.) in a blinded manner. Immunohistochemistry was performed using anti-mouse B220 antibody (BD Biosciences, San Jose, CA) as described previously.¹⁴

Cytokine Analysis and Myeloperoxidase Activity

Mononuclear cells from the spleen (SP), MLN, and colonic lamina propria (LP) were collected as described previ-

ously.¹⁵ CD4⁺ T cells, B cells, and macrophages were separated with CD4, CD19, and CD11b magnetic beads, respectively (Miltenyi Biotech). Cells (10^6 cells) were cultured in flat bottom 96-well culture plates for 48 hours in RPMI 1640 (Sigma-Aldrich, St Louis, MO) with 10% fetal bovine serum and antibiotics/antimycotics in the presence of hamster anti-mouse CD3 and hamster anti-mouse CD28 antibodies (5 μ g/mL; BD Biosciences) for the culture of whole mononuclear cells and T cells, or in the presence of 1 μ g/mL lipopolysaccharides (LPS) from *Escherichia coli* (O111:B4; Sigma-Aldrich) for B cells and macrophages. In coculture assay, 2×10^5 macrophages were cocultured with the same number of B cells in 96-well plates. In separate experiments, macrophages and B cells were cultured while separated by Transwell culture inserts (0.4- μ m pore-size; BD Falcon, Franklin Lakes, NJ). In some experiments, macrophages and B cells were preincubated with lactose or sucrose (Nakalai Tesque Inc., Kyoto, Japan).¹⁶ Macrophages were stimulated with recombinant mouse galectin-1, 3, or 4 (R&D Systems) or vehicle in the presence of LPS. Culture supernatant was collected and cytokine productions of interferon (IFN)- γ , IL-10, IL-17, IL-4, and transforming growth factor- β were determined by enzyme-linked immunosorbent assay (eBioscience, San Diego, CA) according to manufacturer's instructions. Cytokine levels are expressed as the mean \pm standard error of mean of 10^6 cells. Myeloperoxidase activity of the colon was investigated using Myeloperoxidase Chlorination Assay Kit (Cayman Chemical Co, Ann Arbor, MI) according to manufacturers' instructions.

Lectin Microarray

The total pattern of oligosaccharide structures in serum IgG was investigated using an evanescent-field fluorescence-assisted lectin micro array as described previously.¹⁷ Briefly, 45 lectins were immobilized on a glass slide in triplicate, and cellular protein was applied to the array. A fluorescence image of the array was acquired using an evanescent-field fluorescence scanner, GTMASScan III (Nippon Laser & Electronics Lab, Nagoya, Japan).

Flow Cytometric Analysis

Cells were stained with fluorescein isothiocyanate-labeled *Datura stramonium* agglutinin (DSA) or *Ricinus communis* agglutinin 120 (J-Oil Mills, Inc. Tokyo, Japan). Pacific Blue-labeled anti-CD4, phycoerythrin (PE)-labeled anti-CD19, anti-CD25-PE (BD Biosciences), anti-CD11b-fluorescein isothiocyanate, anti-CD11c-PE, and anti-F4/80-PE (eBioscience) were also used. Intracellular IL-10 or Foxp3 was stained using allophycocyanin-labeled anti-IL-10 or Alexa Fluor 488-labeled anti-Foxp3 antibody with Cytofix/Cytoperm (BD Biosciences) according to manufacturer's instructions. These samples were subjected to flow cytometric analysis using a FACS Canto II (BD Biosciences). Data were analyzed using FlowJo software (Tree-Star Inc., Ashland, OR).

Statistical Analysis

Results are expressed as mean \pm standard error of mean. Groups of data were compared by the Mann-Whitney *U* test. Differences were considered statistically significant when *P* < .05.

Results

Serum IgG of *B4galt1*^{+/-} Mice Has an Agalactosyl Pattern Similar to That of Patients With CD

B4GalTI is involved in the biosynthesis of galactose-containing oligosaccharides and is a major galactosyltransferase responsible for selectin ligand biosynthesis among the β 4galactosyltransferase gene family.¹⁸ We first analyzed the IgG oligosaccharide structures of *B4galt1*^{-/-} mice by reverse-phase high-performance liquid chromatography. The peak of the agalactosyl fraction in the fucosylated oligosaccharides (G0F) was smaller than that of the full galactosyl fraction (G2F) in *B4galt1*^{+/+} mice. In marked contrast, the mono-galactosyl (G1F) and G2F oligosaccharide peaks were almost completely absent in *B4galt1*^{-/-} mice (Figure 1A). This finding suggests that

B4GalTI exclusively regulates the attachment of galactose to IgG oligosaccharides. A previous report indicated that B4GalTI enzyme activity in *B4galt1*^{+/-} mice is almost half that in *B4galt1*^{+/+} mice.⁸ In fact, the G2F peak in *B4galt1*^{+/-} mice was much smaller than that in *B4galt1*^{+/+} mice, and the G0F peak in *B4galt1*^{+/-} mice was larger than that of G2F in *B4galt1*^{+/-} mice (Figure 1A). *B4galt1*^{-/-} mice exhibit poor survival and, if born alive, have severely retarded growth.⁸ Therefore, *B4galt1*^{-/-} mice cannot be used for colitis experiments. We realized, however, that the IgG oligosaccharide structures of *B4galt1*^{+/-} mice and *B4galt1*^{+/+} mice resemble those of the patients with CD and healthy subjects, respectively.² We therefore used *B4galt1*^{+/-} mice to investigate the role of agalactosyl oligosaccharides in IBD.

Under specific-pathogen-free conditions, there were no differences in the proportions of the T and B cells and macrophage populations in the SP, MLN, and colonic LP between *B4galt1*^{+/-} and *B4galt1*^{+/+} mice (data not shown). In addition, the cytokine production levels of IFN- γ , IL-17, and IL-10 in the SP were not significantly different between *B4galt1*^{+/-} and *B4galt1*^{+/+} mice (Figure 1B). Cytokine production in MLN or colonic LP was not significantly different between *B4galt1*^{+/-} and *B4galt1*^{+/+} mice, and *B4galt1*^{+/-} mice showed no apparent signs of colitis (data not shown). We confirmed that the baseline immunologic status did not differ between *B4galt1*^{+/-} and *B4galt1*^{+/+} mice.

DSS-Induced Colitis Is Ameliorated in *B4galt1*^{+/-} Mice Compared to *B4galt1*^{+/+} Mice

We next investigated the severity of DSS-induced colitis in *B4galt1*^{+/-} and *B4galt1*^{+/+} mice. *B4galt1*^{+/-} mice that treated with DSS had significantly decreased body weight loss (Figure 2A). In addition, the colons of *B4galt1*^{+/-} mice that received DSS exhibited significantly less shortening and thickening than those of *B4galt1*^{+/+} mice (Figure 2B, C). Consistent with these macroscopic changes, *B4galt1*^{+/-} mice had less severe histologic features of colitis than *B4galt1*^{+/+} mice (Figure 2D). In addition, *B4galt1*^{+/-} mice had significantly lower colitis scores than *B4galt1*^{+/+} mice (Figure 2E). The oligosaccharide structures of IgG, as determined by reversed-phase high-performance liquid chromatography were unchanged before and after the induction of colitis in *B4galt1*^{+/-} and *B4galt1*^{+/+} mice (data not shown).

Increased Production of IL-10 in Macrophages of *B4galt1*^{+/-} Mice

To determine if the amelioration of colitis in *B4galt1*^{+/-} mice is associated with changes in cytokine production, we examined the cytokine production of mononuclear cells isolated from the SP, MLN, and LP of *B4galt1*^{+/+} and *B4galt1*^{+/-} mice with DSS colitis. Although the differences in IFN- γ and IL-17 production between the 2 groups were not significantly different (Figure 3A, B), IL-10 production in the SP, MLN, and LP from

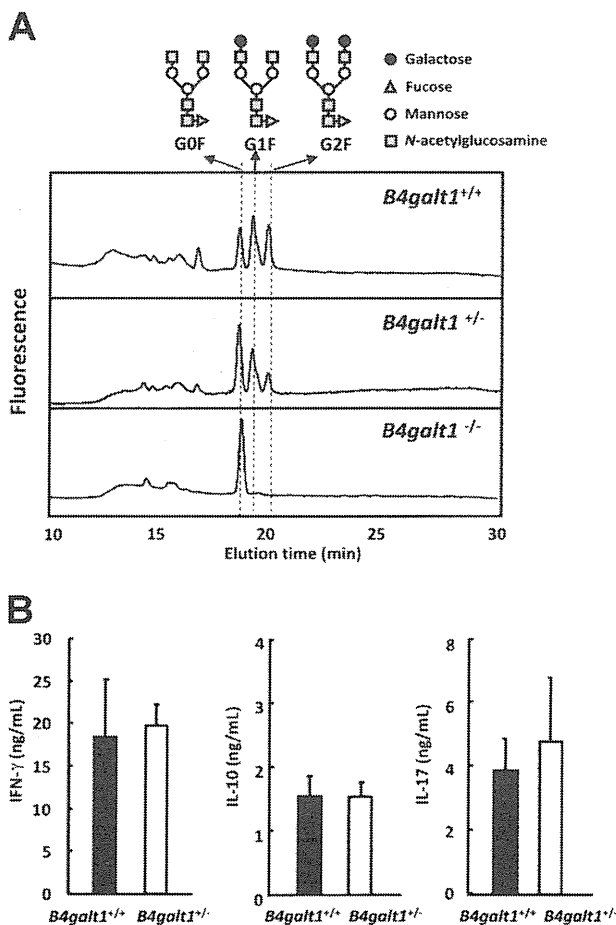


Figure 1. Biochemical and immunologic characteristics of *B4galt1*-deficient mice before the induction of colitis. (A) Oligosaccharide structures attached to serum IgG in *B4galt1*^{+/+}, *B4galt1*^{+/-}, and *B4galt1*^{-/-} mice. Structures of N-linked oligosaccharides were analyzed by reversed-phase high-performance liquid chromatography. (B) Cytokine production of *B4galt1*^{+/+} and *B4galt1*^{+/-} mice. Splenic mononuclear cells were cultured with anti-CD3 and anti-CD28 monoclonal antibodies for 48 hours and cytokine production of IFN- γ , IL-10, and IL-17 in the culture supernatants was determined by enzyme-linked immunosorbent assay. Data are shown as the mean \pm standard error of mean of 4 independent experiments.

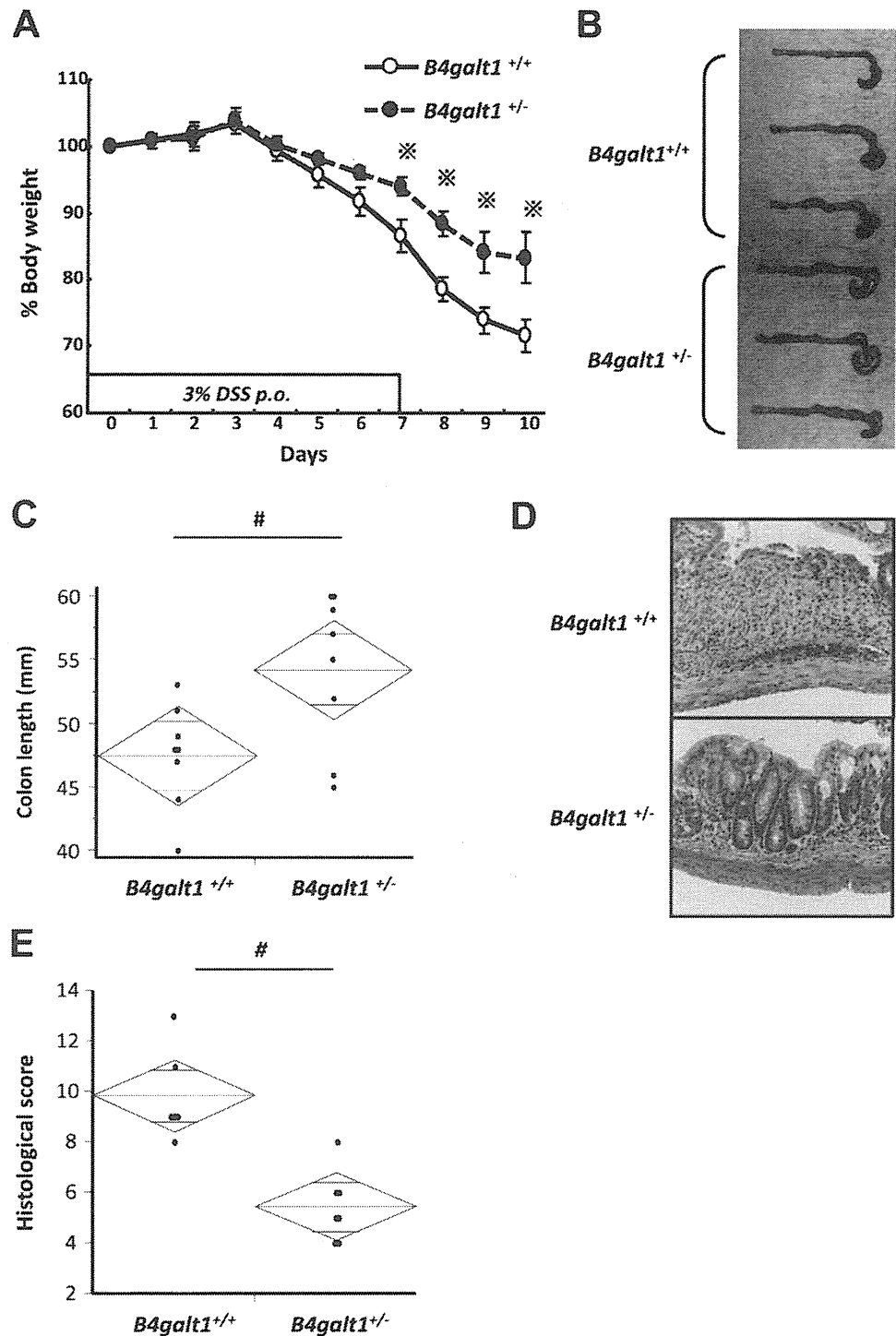


Figure 2. Amelioration of DSS-induced colitis in *B4galt1*^{+/-} mice. (A) Body weight of *B4galt1*^{+/+} and *B4galt1*^{+/-} mice subjected to DSS-induced colitis. Body weight was significantly greater in *B4galt1*^{+/-} mice than *B4galt1*^{+/+} mice. (B) Macroscopic pictures of the colons from *B4galt1*^{+/+} and *B4galt1*^{+/-} mice. (C) Colon length of *B4galt1*^{+/+} and *B4galt1*^{+/-} mice. (D) Representative micrographs of H&E-stained colon. (E) Histologic scores of DSS colitis in *B4galt1*^{+/+} and *B4galt1*^{+/-} mice. Data are shown as mean ± standard error of mean of 8 mice per group. #*P* < .05.

B4galt1^{+/-} mice was significantly higher than that in *B4galt1*^{+/+} mice (Figure 3C). We then purified CD4⁺ T cells, CD19⁺ B cells, and CD11b⁺ macrophages/dendritic cells from the SP of *B4galt1*^{+/-} and *B4galt1*^{+/+} mice to investigate the source of the IL-10 production. IL-10 production by CD11b⁺ cells isolated from *B4galt1*^{+/-} mice was significantly higher than that from *B4galt1*^{+/+} mice, while there was no difference in IL-10 production from

CD4⁺ T cells or from CD19⁺ B cells obtained from *B4galt1*^{+/-} and *B4galt1*^{+/+} mice (Figure 3D). The production of IL-4 and transforming growth factor-β in the colon between the 2 groups was not significantly different (Supplementary Figure 1A, B). When CD11b⁺ cells in colonic LP were intracellularly co-stained with anti-IL-10 antibody, CD11b⁺F4/80⁺ macrophages of *B4galt1*^{+/-} mice produced more IL-10 than those of *B4galt1*^{+/+} mac-